JOURNAL OF
EMERGING INVESTIGATORS

Article

Investigating the effects of glucose reintroduction on acutely starved HeLa cells

Guru Puduru[1], Uma Peddireddy[1], Ammasi Periasamy[2]
[1] Academy of Health and Medical Sciences at Somerset County Vocational and Technical High School, Bridgewater, NJ
[2] Keck Center for Cellular Imaging, University of Virginia, Charlottesville, VA

SUMMARY

Cancer cells exhibit a high degree of metabolic flexibility that distinguishes them from their non-cancerous counterparts. Their reliance on glycolysis, even in oxygen-rich environments, is known as aerobic glycolysis (Warburg effect) and is one of these metabolic adaptations. While the Warburg effect is well-documented, its relationship to glucose availability remains unexplored. Since the Warburg effect drives cancer cells to preferentially consume glucose, acute glucose starvation directly disrupts this, yet, little is known about how HeLa cells metabolically respond when glucose is reintroduced after starvation. Understanding how cancer cells regulate their metabolic phenotype has potential implications for therapy efficacy and resistance. We hypothesized that this re-feeding would push the cells toward rapid activation of their glycolytic pathways, consistent with the Warburg effect. We used two-photon Florescence Light Imaging Microscopy to track redox-sensitive parameters of nicotinamide adenine dinucleotide phosphate (NAD[P]H) and flavin adenine dinucleotide (FAD) in three different fields of view in three states—starved, 20 minutes post–glucose introduction, and 40 minutes post–glucose introduction—for starved and non-starved cells. Most cells shifted toward a more reduced state within the first 20 minutes following glucose reintroduction due to an increase in glycolysis, supporting our initial hypothesis. However, by 40 minutes, the cells exhibited diverging responses: some remained suppressed in regards to aerobic respiration, while others recovered back to oxidative phosphorylation. This indicates that although the initial effect of re-feeding is uniform, over time, there is variance in their metabolic response. Clinically, these findings underscore the importance of accounting for metabolic heterogeneity when treating cancer, as it can completely change resistance and overall efficacy of the therapy.

INTRODUCTION

Cellular metabolism is the foundation of biological function, playing a crucial role in governing the generation and utilization of the energy molecule adenosine triphosphate (ATP), which drives essential cell processes (1). The two main pathways by which cells generate ATP are glycolysis, occurring in the cytoplasm independent of oxygen, and oxidative phosphorylation (OXPHOS), taking place in the mitochondria in an oxygen-dependent process. Although OXPHOS has a substantially higher yield of ATP per glucose molecule (32–38 ATP), cancer cells often favor the much less efficient anaerobic counterpart, glycolysis (2 ATP), a well-documented phenomenon known as the Warburg effect (1, 2). The rapid generation of energy through glycolysis, along with the biological intermediates and substrates it produces, is suggested to be the main reason cancer cells prefer this mechanism over OXPHOS, as both support rapid proliferation (3).

The availability of glucose lies at the heart of this metabolic pathway-determining process. With its role as the primary supply of carbon, glucose contributes to whether cells engage in glycolysis or OXPHOS (4). Additionally, the availability of oxygen is a major factor in this metabolic decision: OXPHOS is dependent on oxygen, while glycolysis is not. In cancer specifically, cells often exhibit increased uptake of glucose, and deprivation of this vital nutrient can lead to severe metabolic stress (1). Previous studies have suggested that cancer cells that are exposed to brief nutrient stress often survive by using their metabolic flexibility—the ability to prioritize OXPHOS or glycolysis when necessary for the cell (4,5). Being able to understand how quickly and to what extent cancer cells recover from stress could provide new perspectives on therapeutic limitations in tumors that heavily rely on glycolysis. Experimentally supplementing starved cancer cells with glucose, combined with quantitative, single-cell analysis, is an especially useful method to test the heterogeneity of response to metabolic stimuli.

To address this, we used two-photon Fluorescence Lifetime Imaging Microscopy (FLIM), a technique that uses the autofluorescent properties of nicotinamide adenosine dinucleotide phosphate (NAD[P]H) and flavin adenine dinucleotide (FAD) to generate data on the metabolic state of the cells being studied. These two cofactors play a vital role in the reduction-oxidation (redox) reactions of glycolysis and OXPHOS, making them the ideal trackers of live-cell metabolism (6). NAD(P)H, a combined signal of NADH and NADPH, reflects cellular redox state; NADH functions as a key electron carrier donating reducing equivalents to the mitochondrial electron transport chain during OXPHOS to drive ATP synthesis, while NADPH primarily supports biosynthetic and antioxidant processes O (6, 7). FAD is reduced to $FADH_2$ during the TCA cycle (notably at succinate dehydrogenase, which is also Complex II of the electron transport chain) and is subsequently oxidized in OXPHOS, directly feeding electrons into the respiratory chain and reflecting mitochondrial oxidative activity (8). FLIM specifically differentiates between the free and enzyme-bound states of NAD(P)H and FAD, which correlate to glycolysis and OXPHOS, respectively (9). Several previous studies have validated that the utility of FLIM-based parameters for the

https://doi.org/10.59720/25-217

evaluation of cellular metabolic states, such as the bound fractions of NAD(P)H-a2% and FAD-a1%, their ratios, and Fluorescence Lifetime Redox Ratio (FLIRR) (10, 11). NAD(P)H-a2% is the proportion of enzyme-bound NAD(P)H and is commonly used as an indicator of oxidative metabolic activity (6, 9). Conversely, FAD-a1% represents the fraction of bound FAD, which decreases when cells shift toward more glycolytic states (9, 12). Combining these metrics into redox ratios provides a more holistic view of cellular metabolism (6, 13). FLIRR, which is the ratio of NAD(P)H-a2% to FAD-a1%, offers a measure of whether the cell is using more glycolytic or oxidative processes to create ATP (9, 12).

In this study, we aimed to use FLIM to track metabolic changes in glucose-deprived HeLa cells over a period of 40 minutes in 20-minute intervals. We used HeLa cells because they were cancer cells and because they were readily available during the study period. Additionally, they have been shown to exhibit the Warburg effect, meaning they favor glycolysis. We hypothesized that re-feeding of glucose would lead to a rapid metabolic recovery, which would be measured using redox-sensitive lifetime parameters of bulk data of the entire field of view (FOV) and segmented data of single cells. We found that the reintroduction of glucose to starved HeLa cells resulted in an early shift toward a reduced intracellular environment consistent with glycolysis. However, after 40 minutes only a subset of cells recovered towards a metabolic profile close to the control—highlighting cellular heterogeneity in metabolism.

RESULTS

To investigate how glucose deprivation affects cellular metabolism and whether metabolic recovery occurs upon re-feeding, we used FLIM to track redox changes in HeLa cells over time. We placed HeLa cells in two environments: a non-starved control and a starved state (in which glucose was deprived). We imaged the non-starved control and the starved group with confocal microscopy. After one hour, we re-fed the glucose to the starved group and imaged them at 20 minutes post-introduction and 40 minutes post-introduction.

This setup allowed for the investigation of how HeLa cells recover metabolically in real time following nutrient stress via glucose starvation. Although studies have found that cancer cells favor glycolysis and exhibit significant metabolic flexibility, the timing and uniformity of this metabolic response after glucose reintroduction are not as well-known (1, 2, 5). Monitoring NAD(P)H and FAD lifetimes pre- and post-introduction of glucose allowed us to measure redox changes and understand their metabolic significance. The segmentation approach gave us insight into cell-to-cell variability as well as the metrics for the whole population.

NADH(P)H and FAD have mean lifetimes (τm) which refer to the weighted averages of their longevity (how long the molecule stays in an excited state) and their fractional contribution (how much each molecule contributes to the overall fluorescence signal). NAD(P)H τm / FAD τm is the ratio of these mean lifetimes and is crucial to quantifying

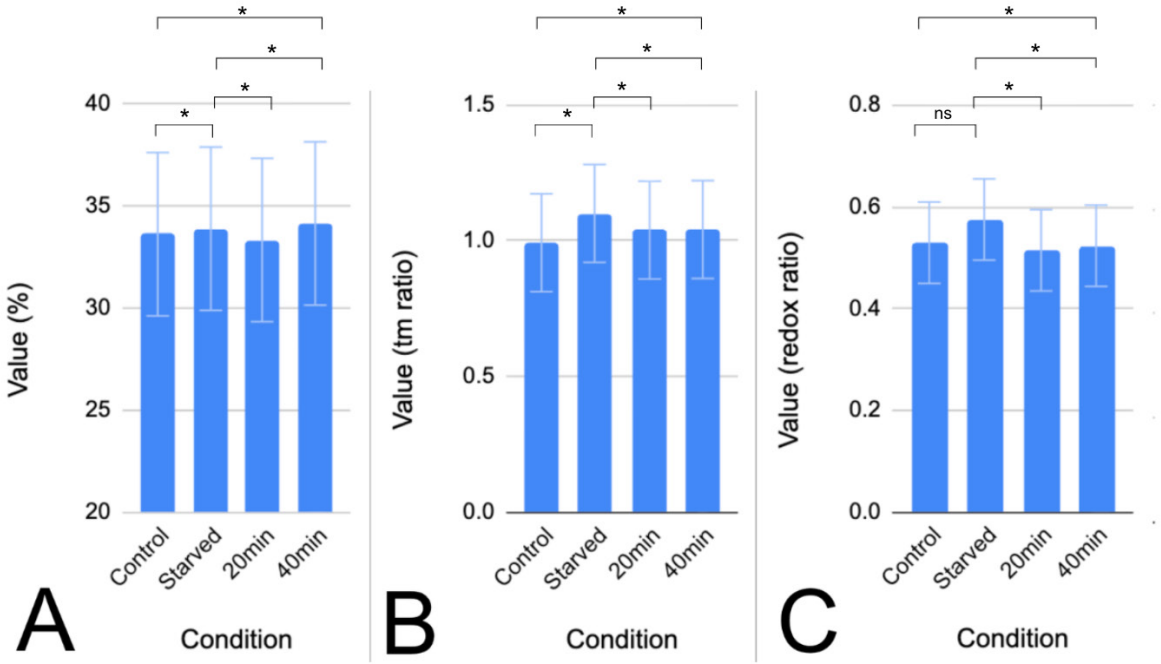

Figure 1. Metabolic changes for whole HeLa cell field of views following glucose reintroduction, measured using fluorescence lifetime imaging microscopy (FLIM). Bar graphs show mean ± SD (standard deviation) for (A) NAD(P)H-a2% (Nicotinamide adenine dinucleotide [phosphate] protein bound fraction), (B) NAD(P)H τm / FAD τm (nicotinamide adenine dinucleotide [phosphate] to flavin adenine dinucleotide mean lifetimes ratio), and (C) FLIRR (florescence lifetime redox ratio) under four treatment conditions: control, starved, 20 minutes post-glucose reintroduction (20 min), and 40 minutes post-glucose reintroduction (40 min). HeLa cells were glucose-starved for one hour using HBSS and re-fed with 25 mM glucose before imaging. Error bars represent standard deviation. Here, metrics were averaged across all segmented single cells combining all three FOVs (n=30). Unpaired, two sample t-tests were conducted on the data. *p<0.05 ("*ns*" is not significant). .

https://doi.org/10.59720/25-217

Parameter	Control average	Starved group average
NAD(P)H τm / FAD τm	0.9 (SD: 0.18)	1.15 (SD: 0.19)
NAD(P)H a2%	48% (SD: 4.1)	33% (SD: 3.9)
FLIRR	0.56 (SD: 0.08)	0.54 (SD: 0.09)

Table 1. Average values of the non-starved control average and starved group as measured by FLIM parameters. Shown are the differences between the average control value of all three FOVs (fields of view) and the average starved group value of all three FOVs for the three FLIM (florescence lifetime imaging microscopy) parameters measured. NAD(P)H τm / FAD τm stands for nicotinamide adenine dinucleotide (phosphate) mean lifetime to flavin adenine dinucleotide mean lifetime ratio. NAD(P)H a2% is the percentage of protein bound nicotinamide adenine dinucleotide (phosphate). FLIRR stands for the florescence lifetime redox ratio.

change in metabolic activity. From the non-starved control to the starved condition, this ratio showed a significant change (p<0.05; **Figure 1**, **Table 1**). Relative to the starved group, the ratio remained significantly decreased at 20 minutes post-reintroduction (p<0.05) and at 40 minutes post-reintroduction (p<0.05; **Figure 1**). In addition, the 40-minute time point differed significantly from the non-starved control (p<0.05; **Figure 1**). Across all three of the FOVs, the NAD(P)H τm / FAD τm ratio decreased from the starved group to 20 minutes post-reintroduction, with the change being most profound in FOV 1 (**Figure 2**). However, a difference arose at 40 minutes: FOV 3's ratio continued to decrease, while FOV 1 and 2 showed partial recovery of the mean lifetimes ratio back to their initial starved levels (**Figure 2**). At the single cell level in FOV 1, 100% (three cells) of the cells' ratio decreased at 20 minutes post-reintroduction, and one out of the three cells (cell 1.01) showed a marginal increase in redox ratio (**Figure 3**). Looking at FOV 2, 67% (six cells) of the cells exhibited a decrease in ratio from the starved state to the first time point, while the remaining cells increased. Among the cells whose mean lifetimes ratio decreased, four increased at 40 minutes, while two remained suppressed (**Figure 3**). FOV 3 was different, however, with 17 out of the 18 cells (94%) exhibited the initial decrease, but none had the later increase at 40 minutes (**Figure 3**). Combining the metrics of all the individual cells, 87% displayed a decrease from the control to 20 minutes, while only 17% exhibited an OXPHOS recovery at 40 minutes (**Table 2**).

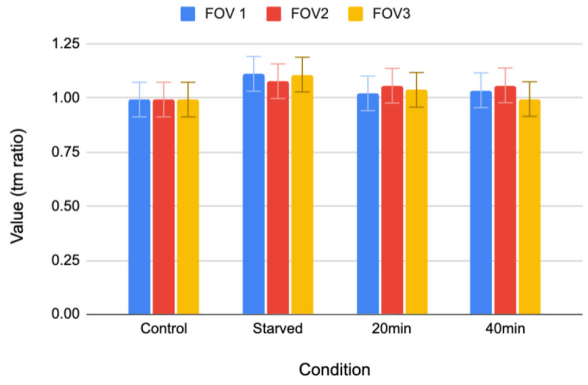

Figure 2. Mean NAD(P)H-to-FAD lifetime ratio changes across fields of view. Mean ± SD (standard deviation) of NAD(P)H τm / FAD τm (nicotinamide adenine dinucleotide [phosphate] mean lifetime to flavin adenine dinucleotide mean lifetime ratio) across three fields of view (FOV1–FOV3) under non-starved (control), glucose-starved (starved), 20 min post-glucose reintroduction (20 min), and 40 min post-glucose reintroduction conditions (40 min). This lifetime ratio reflects relative shifts in NAD(P)H and FAD fluorescence dynamics associated with cellular metabolic state. Sample sizes were n=3 (FOV1), n=9 (FOV2), and n=18 (FOV3). Each bar represents the mean FLIM-derived value across all segmented cells within a given field of view. Error bars represent standard deviation.

NAD(P)H-a2% reflects the percentage of protein-bound NAD(P)H within the selected region of interest (ROI). Protein-bound NAD(P)H is associated with mitochondrial activity and oxidative phosphorylation (OXPHOS). Although NADH and NADPH can be differentiated, it was beyond the objectives of this experiment; thus, our data represent pooled NADH and NADPH, denoted as NAD(P)H. From the non-starved control to the starved condition, a significant decrease in NAD(P)H-a2% was observed (p<0.05; **Figure 1**, **Table 1**). Similarly, glucose reintroduction resulted in significant changes in NAD(P)H-a2% relative to the starved group at both 20 minutes (p<0.05) and 40 minutes (p<0.05), with the 40-minute time point also differing significantly from the non-starved control (p<0.05; **Figure 1**). Observing the whole FOV results, the trends in FOV 1 and FOV 2 were similar to those observed for the NAD(P)H tm / FAD tm ratio, although the changes were less pronounced (**Figure 4**). The whole data for FOV 2 showed a marginal but consistent increase from the starved group to each of the time points (**Figure 4**). Of the cells in FOV 1, all of them showed a decrease in the metric at 20 minutes, while two out of the three increased at 40 minutes. At the single-cell level for FOV 2, 6 out of the 9 cells (67%) decreased in the metric from the starved group to 20 minutes, and 5 out of these 6 then increased in the metric at 40 minutes (**Figure 3**). In FOV 3, 6 out of the 18 cells showed the initial decline in NADH(P)H a2% at 20 minutes and 5 out of the 6 cells (83%) increased at the second time point (**Figure 3**). Overall, 50% of all individual cells showed a decrease in NAD(P)H a2% from starved group to 20 minutes and 40% showed a recovery after 40 minutes (**Table 2**).

Fluorescence lifetime imaging redox ratio (FLIRR) is the ratio of protein-bound NAD(P)H to protein-bound FAD.

https://doi.org/10.59720/25-217

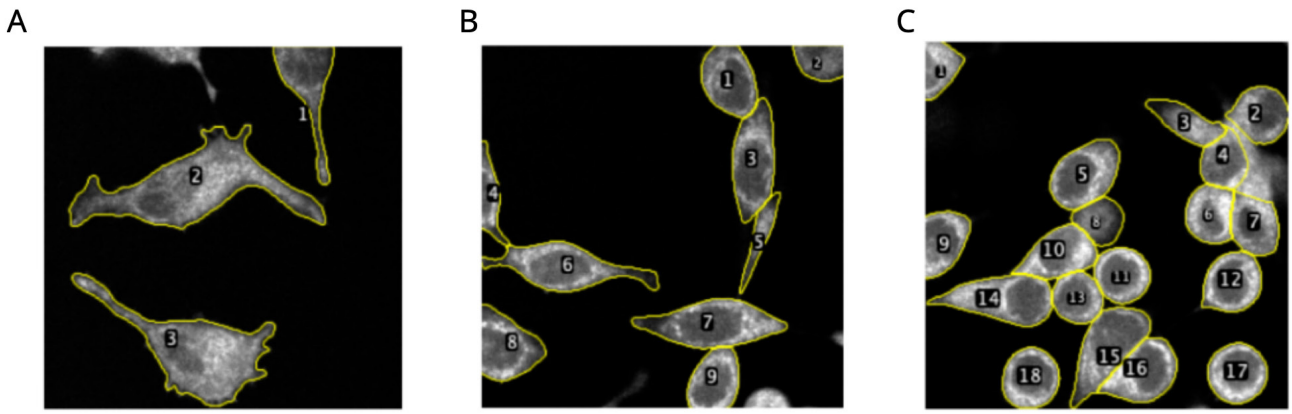

Figure 3. Segmentation of HeLa cells from all fields of view of the starved group using Cellpose and FIJI. Shown are images of three FOVs, (A) is FOV 1, (B) is FOV 2, and (C) is FOV 3, prior to glucose reintroduction. Yellow outlines correspond to regions of interest (ROIs) generated using Cellpose segmentation, which were imported into FIJI for downstream analysis. The segmentation enables tracking of individual cells across all time points during FLIM (florescence lifetime imaging microscopy) analysis.

This metric is widely used and is regarded as one of the best metrics for assessing the metabolic states of cells (7, 8). Once again, in this metric, the value from the starved to the control showed a decrease in value; however, it was not statistically significant (p=0.127; **Figure 1**, **Table 1**). Glucose reintroduction resulted in significant changes relative to the starved group at both 20 minutes (p<0.05) and 40 minutes (p<0.05), with the 40-minute time point also differing significantly from the control (p<0.05; **Figure 1**). Looking at the whole FOVs, all three show a decrease in the ratio from the starved group to 20 minutes, yet only FOV 1 and FOV 2 display cells that recover and have an increase in the ratio at 40 minutes (**Figure 5**). FOV 3 continues to decrease marginally between the two time points (**Figure 5**). Examining FOV 1, all three cells experienced a substantial decrease in FLIRR, and for two out of the three this was followed with an equivalent increase (**Figure 3**). In FOV 2, the FLIRR for six of the cells dropped, and out of these cells, three increased in the ratio at 40 minutes (**Figure 3**). For FOV 3, nine cells displayed a decrease in ratio from the starved group to 20 minutes while five of these cells had a subsequent increase (**Figure 3**). Combining all the individual cell data shows that 60% of the cells had an initial FLIRR decrease FLIRR and 30% had a recovery pattern (**Table 2**).

In culmination, glucose reintroduction post-starvation induced clear, measurable metabolic shifts that could be quantified via multiple FLIM parameters. The NAD(P)H τm / FAD τm ratio decreased across all three FOVs at 20 minutes, with 87% of all single cells showing the same trend. Only 17% showed a subsequent increase by the second time point, indicating that recovery was limited. NAD(P)H-a2% showed a general, initial decrease across the averages of whole FOV data, but only 50% of the individual cells showed this same decrease, while 40% had a recovery. FLIRR displayed a similar pattern with 60% of cells showing a decrease at 20 minutes, followed by 30% of cells displaying a rebound.

DISCUSSION

It is well understood that cells undergoing nutrient deprivation must optimize and change their metabolic

Parameter	% of cells with decreased value at 20 minutes	% of cells increasing value at 40 minutes
NAD(P)H τm / FAD τm	87%	17%
NAD(P)H a2%	50%	40%
FLIRR	60%	30%

Table 2. Summary of cellular metabolic shifts following glucose reintroduction as measured by FLIM parameters. Shown are the percentages of all the cells that decreased initially and/or had a recovery pattern for all of the FLIM (florescence lifetime imaging microscopy) parameters. NAD(P)H τm / FAD τm stands for nicotinamide adenine dinucleotide (phosphate) mean lifetime to flavin adenine dinucleotide mean lifetime ratio. NAD(P)H a2% is the percentage of protein bound nicotinamide adenine dinucleotide (phosphate). FLIRR stands for the florescence lifetime redox ratio.

https://doi.org/10.59720/25-217

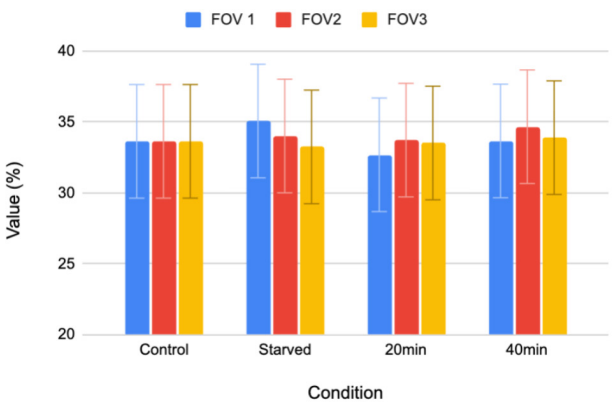

Figure 4. Mean protein-bound NAD(P)H fraction changes across fields of view. Mean ± SD (standard deviation) of NAD(P)H (nicotinamide adenine dinucleotide [phosphate]) a2 (%) measured by fluorescence lifetime imaging microscopy (FLIM) across three independent fields of view (FOV1–FOV3) under four conditions: non-starved (control), glucose-starved (starved), 20 minutes post-glucose reintroduction (20 min), and 40 minutes post-glucose reintroduction (40 min). HeLa cells were glucose-starved for one hour in Hanks' Balanced Salt Solution (HBSS) prior to refeeding with 25 mM glucose. Sample sizes were n=3 (FOV1), n=9 (FOV2), and n=18 (FOV3). Each bar represents the average a2% value across all cells within a FOV. Error bars represent standard deviation.

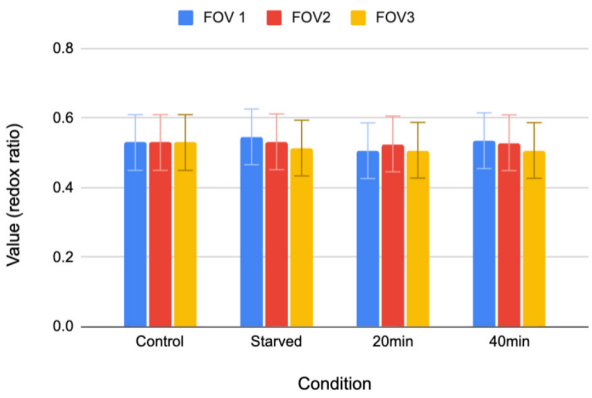

Figure 5. Mean FLIRR (florescence lifetime redox ratio) changes across fields of view. Mean ± SD (standard deviation) of the fluorescence lifetime-based redox ratio (FLIRR) across three independent fields of view (FOV1–FOV3) under non-starved (control), glucose-starved (starved), 20 min post-glucose reintroduction (20 min), and 40 min post-glucose reintroduction conditions (40 min). FLIRR was calculated from FLIM-derived NAD(P)H and FAD signals and reflects relative changes in cellular redox balance. Sample sizes were n=3 (FOV1), n=9 (FOV2), and n=18 (FOV3). Each bar represents the average FLIRR value across all segmented cells within a single field of view. Error bars represent standard deviation.

decision-making to adapt (4). Therefore, inducing deprivation and then reintroduction of an important compound, in this case glucose, offers the unique opportunity to observe and understand this metabolic process firsthand. Our study used FLIM imaging of two important cofactors, NAD(P)H and FAD, to visualize and measure the response of glucose-starved HeLa cells. This study revealed that there is an early shift in metabolic activity coupled with a more variable recovery. The onset of a more reduced intracellular state in the FOVs and in the majority of most cells was likely driven by an increased surge in glycolytic activity. However, the differences in how each cell recovered following this change highlighted the extent of metabolic heterogeneity between cells.

One of the most consistent findings shown throughout the FOVs and the individual cells was the strong response that occurred 20 minutes post-reintroduction. The decrease in mean lifetimes ratio (NAD(P)H τm / FAD τm), matched by declines in both FLIRR and NAD(P)H a2%, suggests a rapid onset of glycolysis (**Figure 2**) (11, 14). This anaerobic process is responsible for the generation of reduced cofactors (e.g. NADH) that alter the environment of the cells, leading to a marked decrease in redox-sensitive FLIM parameters. This interpretation is consistent with previous studies that demonstrated that cells undergoing a glycolytic surge similarly increase in NAD(P)H and create shifts in the FLIM metrics (6). In cells that are known to exhibit the Warburg effect, such as HeLa cells, the glycolytic pathways are, most likely, already primed for activation, which can accelerate this transition (1).

Following this mostly uniform decision observed across the FOVs and cells to initiate glycolysis were more varied results that clearly indicate heterogeneity. While some of the cells began to rebound in parameter values back to their pre-glucose-reintroduction state by the 40-minute mark, others remained reduced or continued trending downward (**Figure 1**). This divergence suggests that while almost all of the cells registered the same reaction to glucose, with an increase in glycolysis, the ability to restart the OXPHOS appears more selective. The nature of this phenomenon can be explained by several possible theories. First, there could be variability in mitochondrial readiness. Cells that displayed deeper, more prolonged mitochondrial suppression during the starvation period may have required a lengthier time to rebuild the membrane potential and enzyme complexes that are key to OXPHOS. On the other hand, those that maintained more mitochondrial function could have been quicker to initiate oxidative phosphorylation to the level at which it was before glucose was reintroduced. This could provide a potential explanation as to why the cells in FOV 1 and FOV 2 had markedly higher rates of OXPHOS recovery than those in FOV 3 (14, 15).

Differences in the glucose metabolism may also contribute to a varied recovery of OXPHOS in the cells that were studied. Although the initial decline in redox state suggests that a majority of the cells had responded metabolically to glucose reintroduction, the frequency and extent of this response likely varied between cells. For example, a variability in glucose transporter expression (such as GLUT1) may result in prolonged glycolysis in some cells, which then delays mitochondrial restoration (16). Cells that have sustained glycolytic metabolism may maintain elevated NADH, reinforcing a reduced redox state even when energy availability is sufficient. Therefore, longer and higher levels of glycolytic activity in some cells could persist despite adequate conditions for OXPHOS to take place. Along with this, some cells could remain in a reduced state for longer periods as a potential adaptive strategy. As mentioned before, glycolysis provides cancer cells with benefits beyond speed such as providing molecules for the biosynthesis required to proliferate

https://doi.org/10.59720/25-217

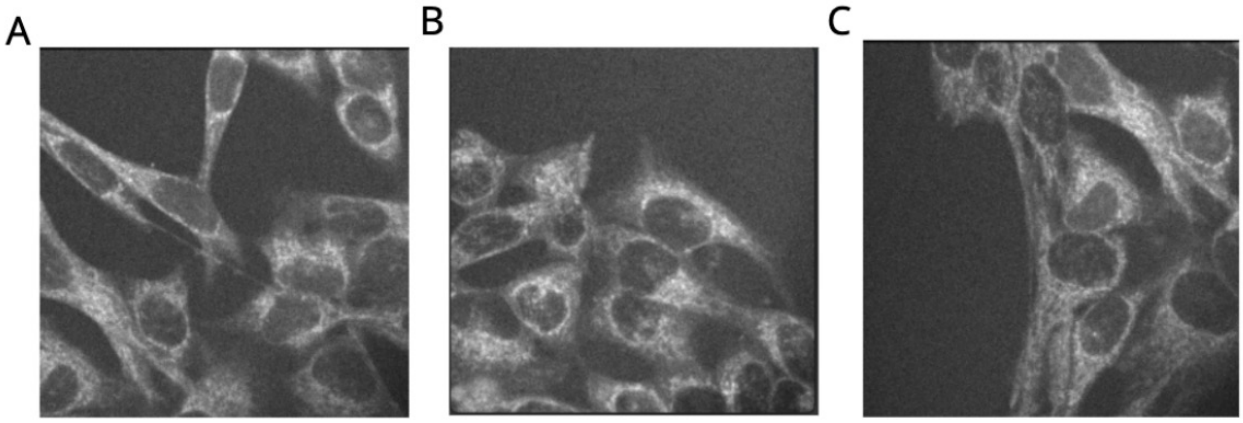

Figure 6. Non-segmented HeLa cells in a non-starved state using FIJI. Shown are images of HeLa cells that were imaged in their non-starved state. There are three FOVs (fields of view), (A) is FOV 1-normal, (B) is FOV 2-normal, and (C) is FOV 3-normal. These FOVs do not correspond to the same FOVs used in the experimental batch and were obtained from a different population of cells. Images are shown as TIFF files processed in FIJI.

(17). In the context of recovery from stress, being in a state of glycolysis may reflect a protective mechanism in these cells by avoiding the oxidative load associated with mitochondrial reactivation. Another important note was that there were differences in how the cells in each FOV acted that could be attributed to the number of cells. FOV 1 had fewer cells than FOV 3 and showed an overall greater degree of reduction and increase in numerical quantities of metrics measured. When there are more cells present, cell-communication could allow each individual cell to be more resistant (15, 17).

The patterns observed in this study are biologically meaningful as they highlight the fact that cellular populations can be unified in an immediate response but also underscore the individuality in how they manage recovery in the long term. Specifically, this has important implications for cancer metabolism and treatment. Therapeutic strategies that target glycolysis during early, synchronized shifts after nutrient stress may be effective (18). Aims of blocking mitochondrial recovery may need to be delayed and should account for high variability in the rebound phases. Along with this, identification of cells that don't recover at all can serve as a biomarker of metabolic resilience within a tumor. Studies in the future would benefit from combining FLIM with reactive oxygen species sensors, ATP reporters, or mitochondrial dyes that could clarify whether the failures in recovery are due to energetic, redox, or structural issues.

Our study has several limitations. Firstly, the cell population used was an immortalized line of cervical cancer (HeLa), and therefore the results may not be generalized to other kinds of cancer. Additionally, the starvation period was not optimized via any mathematical or previously used model. Furthermore, the time points for our study were restricted to 20 and 40 minutes, so we could have missed significant events occurring outside of that timeframe. Finally, the number of FOVs and cells chosen could have been increased to create results that were more accurate.

In conclusion, our study reveals how the reintroduction of glucose to starved HeLa cells produces immediate, consistent glycolytic changes, but more variable recovery responses. Nearly all the cells shifted to a reduced metabolic state using glycolysis, but only a small fraction returned to their initial state at the 40-minute mark. There could be many reasons behind this observation, such as mitochondrial readiness, differences in nutrient uptake, and tradeoffs between OXPHOS and glycolysis. These findings show that redox-based, segmented cell imaging and analysis provide important insights into diversity of cellular responses to stress, a necessary step toward fully understanding the nature of cancer cell metabolism.

MATERIALS AND METHODS

Cell Culture

HeLa cells were cultured in a high-glucose Dulbecco's Modified Eagle Medium (DMEM from Life Technologies) and supplemented with 10% cosmic calf serum (Hyclone) and 4 mM sodium pyruvate (Life Technologies). The cells were starved for one hour using Hanks' Balanced Salt Solution. They were re-fed in a Flurobrite 25 mM glucose solution (Life Technologies). For imaging, cells were seeded onto 25 mm round No. 1.5 glass coverslips (Thermo Scientific). The live cancer cells were exclusively handled by Dr. Vijay Kumar Sagar of the University of Virginia due to biosafety requirements (19).

Instrumentation

A Zeiss LSM-780 confocal/multiphoton microscopy system that included a motorized stage was used for automated scanning, equipped with a Chameleon Vision-II (Coherent Inc.) Ti:sapphire laser and an inverted Axio Observer. There were also three HPM 100-40 hybrid GaAsP detectors from Becker & Hickl that were attached to the non-descanned port of the microscope using adapters from Zeiss. The single photon counting module (SPCM) software from Becker & Hickl was used to acquire the images. A Zeiss stage was motorized on all three axes to ensure that the frames captured were in the exact same position across treatment. A humidified blood-gas mixture was used to keep the specimens at a temperature of 37°C. A Zeiss 40x NA 1.3 oil apochromatic

objective lens was used. Each image was taken within 45 seconds to 60 seconds of turning on the laser using a safe power at the specimen plane to avoid photobleaching with a simultaneous excitation of 800 nm (19, 20).

FLIM Parameter Fitting and Image Processing

The FLIM output from the Zeiss LSM-780 was imported into the single photon counting (SPC) Image software developed and sold by Becker & Hickl. The cells were not stained or treated with any reagents because NAD(P)H and FAD are naturally autofluorescent metabolic cofactors. Fluorescence lifetimes were measured using two-photon excitation and time-correlated single photon counting (TCSPC), which generates a decay curve for each pixel. SPC Image fit these curves to a bi-exponential model to obtain parameters such as NAD(P)H-a2% (the fractional contribution of protein-bound NAD(P)H). FLIRR was calculated as the ratio of the mean lifetimes of NAD(P)H and FAD, providing a label-free readout of metabolic state. The data was then taken into the Cellpose software to segment the FOVs into their individual cells. This was followed by matching of frames to ensure that the same cells were analyzed in parallel in each treated image using FIJI (19).

FLIM Data Acquisition and Analysis

The fitted data and the ROI .zip files that outlined the individual cells were analyzed in FIJI through a plugin and then exported into a custom Python script known as FLIM Analyzer (https://github.com/uvaKCCI/flimanalyzer). This data resulted in a .txt file that the Python script plotted into bar charts. The data were then moved from Python to Google Sheets to perform statistical analysis (using an unpaired, two-sample t-test) and to create graphs. The threshold of significance in this study was a *p* value of under 0.05 (19).

ACKNOWLEDGMENTS

The authors would also like to thank Mr. Horst Wallrabe for helping us learn data analysis and the process of writing a scientific manuscript. The authors would like to thank Ms. Katherin Christopher for culturing the HeLa cells and Dr. Vijay Kumar Sagar for helping us with the instrumentation and cell culturing due to the biosafety requirements set in place on live cancer cells. We would like to mention Ms. Nila Elangovan for assistance during the initial imaging process. The methodology for this experiment was created by referencing the work of Drs. Shagufta, Siller, Zhang, and Periasamy. We would also like to acknowledge FIJI-ImageJ, the custom FLIM Analyzer script, the Cellpose software, and the Keck Center allowing us to adequately analyze the cells in this study.

Received: July 29, 2025
Accepted: January 13, 2026
Published: July, 2026

REFERENCES

1. Liberti, Maria V. and Jason W. Locasale. “The Warburg Effect: How Does It Benefit Cancer Cells?” *Trends in Biochemical Sciences*, vol. 41, no. 3, Mar. 2016, p. 211–218. https://doi.org/10.1016/j.tibs.2015.12.001.
2. Warburg, Otto. “On the Origin of Cancer Cells.” *Science*, vol. 123, no. 3191, 27 Feb. 1956, p. 309–314. https://doi.org/10.1126/science.123.3191.309.
3. Vander Heiden, Matthew G., *et al.* “Understanding the Warburg Effect: The Metabolic Requirements of Cell Proliferation.” *Science*, vol. 324, no. 5930, 22 May 2009, p. 1029–1033. https://doi.org/10.1126/science.1160809.
4. Palm, Wilhelm. “Metabolic Plasticity Allows Cancer Cells to Thrive under Nutrient Starvation.” *Proceedings of the National Academy of Sciences of the United States of America*, vol. 118, no. 14, 6 Apr. 2021, e2102057118. https://doi.org/10.1073/pnas.2102057118.
5. Hensley, Christopher T., *et al.* “Metabolic Heterogeneity in Human Lung Tumors.” *Cell*, vol. 164, no. 4, 11 Feb. 2016, p. 681–694. https://doi.org/10.1016/j.cell.2015.12.034.
6. Blacker, Thomas S., *et al.* “Investigating Mitochondrial Redox State Using NADH and NADPH Autofluorescence.” *Free Radical Biology & Medicine*, vol. 100, Jan. 2016, p. 53–65. https://doi.org/10.1016/j.freeradbiomed.2016.08.010.
7. Hang, Yang, *et al.* "NAD+ Metabolism: Pathophysiologic Mechanisms and Therapeutic Potential." *Signal Transduction and Targeted Therapy*, vol. 5, 7 Oct. 2020, p. 227. https://doi.org/10.1038/s41392-020-00311-7.
8. Martínez-Reyes, Inmaculada, and Navdeep S. Chandel. "Mitochondrial TCA Cycle Metabolites Control Physiology and Disease." *Nature Communications*, vol. 11, 3 Jan. 2020, p. 102. https://doi.org/10.1038/s41467-019-13668-3.
9. Bhatt, Deepanshi, *et al.* "Investigation of Mitochondrial Metabolic Response to Doxorubicin in Prostate Cancer Cells: An NADH, FAD and Tryptophan FLIM Assay." *Scientific Reports*, vol. 7, 5 Sept. 2017, p. 10451. https://doi.org/10.1038/s41598-017-10856-3.
10. Bird, Damian K., *et al.* “Metabolic Maping of MCF10A Human Breast Cells via Multiphoton Fluorescence Lifetime Imaging of the Coenzyme NADH.” *Cancer Research*, vol. 65, no. 19, 1 Oct. 2005, p. 8766–8773. https://doi.org/10.1158/0008-5472.CAN-04-3922.
11. Cao, Ruofan, *et al.* “Single-Cell Redox States Analyzed by Fluorescence Lifetime Metrics and Tryptophan FRET Interaction with NAD(P)H.” *Cytometry Part A*, vol. 95, no. 1, Jan. 2019, p. 110–121. https://doi.org/10.1002/cyto.a.23711.
12. Shirmanova, Marina V., *et al.* "Simultaneous NAD(P)H and FAD Fluorescence Lifetime Microscopy of Long UVA-Induced Metabolic Stress in Reconstructed Human Skin." *Scientific Reports*, vol. 11, 12 Nov. 2021, p. 22222. https://doi.org/10.1038/s41598-021-00126-8.
13. Blacker, Tomás S., *et al.* "Separating NADH and NADPH Fluorescence in Live Cells and Tissues Using FLIM." *Nature Communications*, vol. 5, 4 June 2014, p. 3936. https://doi.org/10.1038/ncomms4936.
14. Bluemel, Gabriele, *et al.* “PCK2 Opposes Mitochondrial Respiration and Maintains the Redox Balance in Starved Lung Cancer Cells.” *Free Radical Biology & Medicine*, vol. 176, Dec. 2021, p. 34–45. https://doi.org/10.1016/j.freeradbiomed.2021.09.007.
15. Raut, Ganesh Kumar, *et al.* “Glucose Starvation-Induced Oxidative Stress Causes Mitochondrial Dysfunction and Apoptosis via Prohibitin 1 Upregulation in Human Breast Cancer Cells.” *Free Radical Biology & Medicine*, vol.

145, Dec. 2019, p. 428–441. https://doi.org/10.1016/j.freeradbiomed.2019.09.020.
16. Carvalho, Kátia C.,*et al.* "GLUT1 Expression in Malignant Tumors and Its Use as an Immunodiagnostic Marker." *Clinics (São Paulo)*, vol. 66, no. 6, 2011, p. 965–972. https://doi.org/10.1590/S1807-59322011000600008.
17. Ward, Patrick S., *et al.* "Metabolic Reprogramming: A Cancer Hallmark Even Warburg Did Not Anticipate." *Cancer Cell*, vol. 21, no. 3, 20 Mar. 2012, p. 297–308. https://doi.org/10.1016/j.ccr.2012.02.014.
18. Hay, Nissim. "Reprogramming Glucose Metabolism in Cancer." *Nature Reviews Cancer*, vol. 16, no. 10, Oct. 2016, p. 635–649. https://doi.org/10.1038/nrc.2016.97.
19. Zhang, Jiaxin, *et al.* "Measuring Metabolic Changes in Cancer Cells Using Two-Photon Fluorescence Lifetime Imaging Microscopy and Machine-Learning Analysis." *Journal of Biophotonics*, vol. 18, no. 1, Jan. 2025, e202400426. https://doi.org/10.1002/jbio.202400426.
20. Cao, Ruofan, *et al.* "Multiphoton FLIM Imaging of NAD(P)H and FAD with One Excitation Wavelength." *Journal of Biomedical Optics*, vol. 25, no. 1, Jan. 2020, p. 1–16. https://doi.org/10.1117/1.JBO.25.1.014510.
21. Stincone, Anna, *et al.* "The Return of Metabolism: Biochemistry and Physiology of the Pentose Phosphate Pathway." *Biological Reviews*, vol. 90, no. 3, Aug. 2015, p. 927–963. https://doi.org/10.1111/brv.12140.
22. Skala, Melissa C., *et al.* "In Vivo Multiphoton Fluorescence Lifetime Imaging of Protein-Bound and Free Nicotinamide Adenine Dinucleotide in Normal and Precancerous Epithelia." *Journal of Biomedical Optics*, vol. 12, no. 2, Mar. 2007, p. 024014. https://doi.org/10.1117/1.2717503.
23. Georgakoudi, Irene, *et al.* "Optical Imaging Using Endogenous Contrast to Assess Metabolic State." *Annual Review of Biomedical Engineering*, vol. 14, Aug. 2012, p. 351–367. https://doi.org/10.1146/annurev-bioeng-071811-150108.
24. Honkoop, Hessel, *et al.* "Single-Cell Analysis Uncovers That Metabolic Reprogramming by ErbB2 Signaling Is Essential for Cardiomyocyte Proliferation in the Regenerating Heart." *eLife*, vol. 8, 23 Dec. 2019, p. e50163. https://doi.org/10.7554/eLife.50163.
25. Karrobi, Kavon, *et al.* "Fluorescence Lifetime Imaging Microscopy (FLIM) Reveals Spatial-Metabolic Changes in 3D Breast Cancer Spheroids." *Scientific Reports*, vol. 13, no. 1, 3 Mar. 2023, 3624. https://doi.org/10.1038/s41598-023-30403-7.
26. Gohil, Vishal M., *et al.*. "Nutrient-Sensitized Screening for Drugs That Shift Energy Metabolism from Mitochondrial Respiration to Glycolysis." *Nature Biotechnology*, vol. 28, no. 3, Mar. 2010, p. 249–255. https://doi.org/10.1038/nbt.1606.
27. Sharick, Joe T.,*et al.* "Protein-Bound NAD(P)H Lifetime Is Sensitive to Multiple Fates of Glucose Carbon." *Scientific Reports*, vol. 8, no. 1, 3 Apr. 2018, 5456. https://doi.org/10.1038/s41598-018-23691-x.
28. Periasamy, A., and R. M. Clegg. "What, Why, How—A Prologue." FLIM Microscopy in Biology and Medicine, edited by A. Periasamy and R. M. Clegg, 1st ed., Chapman and Hall/CRC, 2009, pp. 3–34. https://doi.org/10.1201/9781420078916.
29. Periasamy, A., and R. M. Clegg. "Principles of Fluorescence for Quantitative Fluorescence Microscopy." FLIM Microscopy in Biology and Medicine, edited by A. Periasamy and R. M. Clegg, 1st ed., Chapman and Hall/CRC, 2009, pp. 35–64. https://doi.org/10.1201/9781420078916.
30. Periasamy, A., and R. M. Clegg. "Visible Fluorescent Proteins for FRET-FLIM." FLIM Microscopy in Biology and Medicine, edited by A. Periasamy and R. M. Clegg, 1st ed., Chapman and Hall/CRC, 2009, pp. 65–90. https://doi.org/10.1201/9781420078916